Received: 6 July 2018 | Accepted: 27 August 2018

DOI: 10.1111/gbi.12317

ORIGINAL ARTICLE

WILEY gebiology

A sluggish mid-Proterozoic biosphere and its effect on Earth's redox balance

Kazumi Ozaki[1,2,3] | Christopher T. Reinhard[1,2] | Eiichi Tajika[4]

[1]School of Earth and Atmospheric Sciences, Georgia Institute of Technology, Atlanta, Georgia

[2]NASA Astrobiology Institute, Alternative Earths Team, Mountain View, California

[3]NASA Postdoctoral Program, Universities Space Research Association, Columbia, Maryland

[4]Department of Earth and Planetary Science, Graduate School of Science, The University of Tokyo, Bunkyo-ku, Japan

Correspondence
Kazumi Ozaki, School of Earth and Atmospheric Sciences, Georgia Institute of Technology, Atlanta, GA 30332, USA.
Email: kazumi.ozaki@sci.toho-u.ac.jp

Present address
Kazumi Ozaki, Department of Environmental Science, Toho University, Chiba, Japan.

Funding information
Japan Society for the Promotion of Science, Grant/Award Number: JP16K05618 and JP25870185; NASA Astrobiology Institute, Grant/Award Number: NNA15BB03A; Alfred P. Sloan Foundation, Grant/Award Number: FR-2015-65744

Abstract

The possibility of low but nontrivial atmospheric oxygen (O_2) levels during the mid-Proterozoic (between 1.8 and 0.8 billion years ago, Ga) has important ramifications for understanding Earth's O_2 cycle, the evolution of complex life and evolving climate stability. However, the regulatory mechanisms and redox fluxes required to stabilize these O_2 levels in the face of continued biological oxygen production remain uncertain. Here, we develop a biogeochemical model of the C-N-P-O_2-S cycles and use it to constrain global redox balance in the mid-Proterozoic ocean–atmosphere system. By employing a Monte Carlo approach bounded by observations from the geologic record, we infer that the rate of net biospheric O_2 production was $3.5^{+1.4}_{-1.1}$ Tmol year^{-1} (1σ), or ~25% of today's value, owing largely to phosphorus scarcity in the ocean interior. Pyrite burial in marine sediments would have represented a comparable or more significant O_2 source than organic carbon burial, implying a potentially important role for Earth's sulphur cycle in balancing the oxygen cycle and regulating atmospheric O_2 levels. Our statistical approach provides a uniquely comprehensive view of Earth system biogeochemistry and global O_2 cycling during mid-Proterozoic time and implicates severe P biolimitation as the backdrop for Precambrian geochemical and biological evolution.

KEYWORDS
biogeochemical cycles, oxygen cycle, proterozoic

1 | INTRODUCTION

The modern Earth's biosphere generates copious amounts of molecular oxygen (O_2)—the results of which can be seen from the uppermost atmosphere to the deepest reaches of the ocean. This remarkable abundance of O_2 is ultimately sustained by the activity of oxygenic photosynthesis, representing a critical control on the evolution of surface environments throughout the Earth's history and the emergence and expansion of biological complexity. Although this history has been reconstructed in broad strokes, significant gaps remain in our understanding of the cause-and-effect relationships and quantitative features regulating Earth system evolution. For example, geochemical proxies are consistent with a broad range of atmospheric O_2 levels during Earth's middle age (the "mid-Proterozoic," between ~1.8 and 0.8 billion years ago, Ga) (Holland, 1984; Kump, 2008; Lyons, Reinhard, & Planavsky, 2014) and are themselves agnostic as to the mechanisms regulating the global O_2 cycle. From this point of view, unravelling the global O_2 budget during mid-Proterozoic time is crucial as a window into planetary O_2 cycling, early eukaryotic evolution and the ultimate rise of animals.

A range of sedimentological and geochemical observations (Cole et al., 2016; Hardisty et al., 2017; Planavsky et al., 2014; Tang, Shi, Wang,

& Jiang, 2016) has suggested the intriguing possibility that atmospheric O_2 levels remained low (<0.1%–10% of the present atmospheric level, PAL) for much of mid-Proterozoic time, yet the mechanism(s) and redox fluxes involved in maintaining such low O_2 levels remain enigmatic. In particular, the fragmentary nature of Earth's Precambrian rock record and uncertainty in isotope mass balance models (Bjerrum & Canfield, 2004; Hayes & Waldbauer, 2006; Krissansen-Totton, Buick, & Catling, 2015; Schrag, Higgins, Macdonald, & Johnston, 2013) has resulted in concomitant uncertainties in Earth's evolving O_2 budget. One simple explanation would be a less active oxygenic biosphere, perhaps mediated through limitation of oxygenic photosynthesis by major nutrients (P and N) (Bjerrum & Canfield, 2002; Derry, 2015; Laakso & Schrag, 2014; Planavsky et al., 2010; Reinhard et al., 2017) and bioessential trace elements (Anbar & Knoll, 2002; Scott et al., 2008). However, fully elucidating the factors linking nutrient availability, the size and scope of Earth's biosphere, and atmospheric O_2 during the mid-Proterozoic requires an explicitly quantitative biogeochemical framework for O_2 production and consumption that satisfies global redox balance and is consistent with constraints from the geologic record.

2 | METHODS

Here, we employ a novel biogeochemical model of the ocean–atmosphere system (CANOPS) with the goal of statistically constraining the rate of biotic O_2 production and the attendant

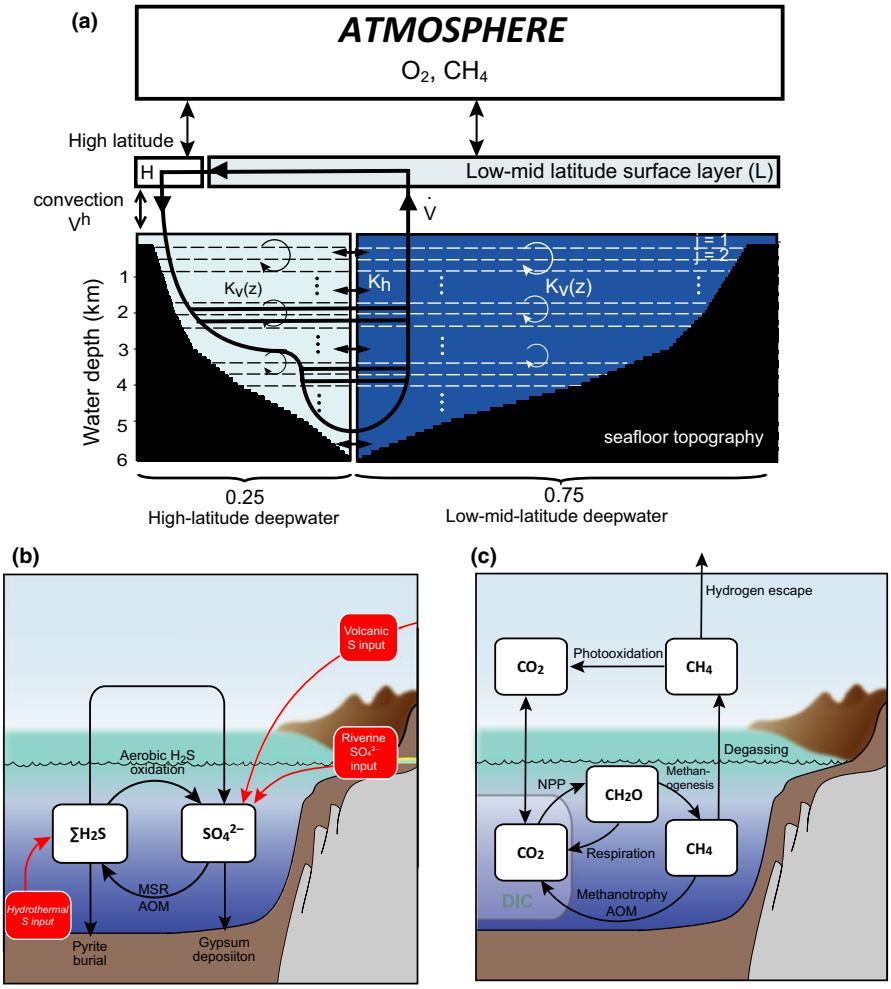

FIGURE 1 Model schematic. (a) CANOPS model configuration. The parameters regarding geometry and water transport are tabulated in Supporting information Table S3. (b) Global sulphur cycle schematic. Two sulphur species (SO_4^{2-} and ΣH_2S) are transformed each other via microbial sulphate reduction (MSR), AOM and sulphide oxidation reactions. Riverine and subaerial/submarine volcanic inputs are the primary source of sulphur to the ocean, and the burial of pyrite and gypsum in marine sediments is the primary sink. It is assumed that hydrogen sulphide escaping from the ocean to the atmosphere is completely oxidized and returns to the ocean as sulphate. The organic sulphur cycle is ignored in this study. (c) Global CH_4 cycle schematic. The model includes CH_4 generation via methanogenesis and its oxidation reactions via methanotrophy and AOM in the ocean interior, as well as CH_4 degassing flux to the atmosphere and its photooxidation. The rates of CH_4 photooxidation and hydrogen escape to space are calculated according to the parameterizations proposed by Goldblatt, Lenton, and Watson (2006). No input of abiotic CH_4 via continental hydrothermal systems is accounted for because previous estimate of modern value (<0.3 Tmol year^{-1}; (Fiebig, Woodland, D'Alessandro, & Püttmann, 2009)) is negligible relative to the biological flux, although we realize that it would play a role in the global redox budget [Colour figure can be viewed at wileyonlinelibrary.com]

large-scale biogeochemistry of the mid-Proterozoic Earth system. CANOPS is a 1-D (vertically resolved) intermediate complexity box model of ocean biogeochemistry (Ozaki & Tajika, 2013; Ozaki, Tajima, & Tajika, 2011; Reinhard et al., 2017) (see Figure 1 and Supporting information Methods for a further explanation). We use constraints from the geologic record to perform a Monte Carlo analysis of significant biogeochemical fluxes based on a wide range of values for poorly constrained control parameters (see Table 1 and Supporting information Methods), which offers a comprehensive and robust quantitative picture of Earth system biogeochemistry. In this study, we focus on eight key parameters that play a quantitatively important role in the marine carbon, phosphorus and sulphur budgets. For the sake of objective analysis, we adopt uniform (noninformative) prior distributions, except for crustal sulphur reservoirs, for which Gaussian probability density functions were assumed. Each simulation was run long enough to establish a steady state, which was verified by looking at the evolution of the concentration of chemical species and the sulphur budget over tens of millions of years.

We sample and statistically analyse a subset of model runs that yield seawater sulphate (SO_4^{2-}) concentrations between 0.1 and 1 mM, as constrained by the stable isotope record of Proterozoic marine sedimentary rocks (Luo et al., 2015; Lyons & Gill, 2010; Planavsky, Bekker, Hofmann, Owens, & Lyons, 2012; Scott et al., 2014). Of the total ~22,000 simulations performed, 3,342 simulations met this criterion (the "All" scenario of Supporting information Table S5). In our "Low O_2" and "High O_2" scenarios, we assumed lower upper limits for $f_{erosion}$ and K_{MSR}, yielding 621 and 308 simulations for analysis. We tracked the median value of J_{oc}^{bur} and J_{py}^{bur} to evaluate convergence—whether the sampling procedure was run for long enough to obtain the stationary distribution (Supporting information Figure S1). Like all geochemical constraints, mid-Proterozoic SO_4^{2-} levels are subject to some degree of uncertainty. However, the magnitude of uncertainty is significantly less than that of other poorly constrained boundary conditions, and in any case, our principal conclusions are not strongly affected by relaxing this constraint. For example, the upper bound could be higher (Kah, Lyons, & Frank, 2004), but in this case the model retrieves parameter combinations that predict lower biological productivity, strengthening our core arguments. This arises as a result of the need to suppress microbial sulphate reduction (MSR) (and subsequent pyrite precipitation) in order to achieve higher [SO_4^{2-}], which is most straightforwardly achieved by a decrease in the availability of organic matter for MSR.

3 | RESULTS AND DISCUSSION

3.1 | Limited O_2 production in Proterozoic oceans

The most striking result of our statistical analysis is the need for a limited rate of O_2 production from organic carbon and pyrite sulphur burial in order to remain consistent with existing constraints on seawater [SO_4^{2-}]. For our "Low O_2" scenario, the posterior probability distribution for the global rate of organic carbon burial (J_{oc}^{bur}) suggests a mid-Proterozoic rate of ~0.5–2.5 Tmol C $year^{-1}$, with a median of $1.10^{+0.93}_{-0.64}$ Tmol C $year^{-1}$ (1σ) and a 95% credible interval of 0.20–3.41 Tmol C $year^{-1}$ (Figure 2a blue). These fluxes are well below estimates of marine organic carbon burial for the modern (10.5–13.3 Tmol C $year^{-1}$) (Berner, 1982; Burdige, 2005; Muller-Karger et al., 2005), Holocene (11.4 Tmol C $year^{-1}$) (Wallmann et al., 2012) and Quaternary (12.92 Tmol C $year^{-1}$) (Wallmann et al., 2012). On the other hand, our model estimates the global burial rate of pyrite sulphur (J_{py}^{bur}) at $1.18^{+0.26}_{-0.26}$ Tmol S $year^{-1}$ (1σ)

TABLE 1 Parameter ranges used in our Monte Carlo analysis

	Scenario		
Sampled parameters	**Low O_2 (n = 621)**	**High O_2 (n = 308)**	**Sampling method**
Atmospheric oxygen level, pO_2 (PAL)	0.01%–1%	1%–10%	Log uniform
Half-saturation constant for MSR, K_{MSR} (mM)	0.002–0.5	0.002–0.5	Log uniform
Riverine reactive P input rate, R_P (normalized)[a]	0%–200%	0%–200%	Uniform
Phosphorus scavenging efficiency, σ_{scav}	0–1	0–1	Uniform
Total crustal sulphur reservoir size, S_{py} + S_{gyp} (10^{18} mole)	400 ± 100 (1σ)	400 ± 100 (1σ)	Gaussian
Crustal gypsum sulphur reservoir size, S_{gyp} (10^{18} mole)	50 ± 25 (1σ)	50 ± 25 (1σ)	Gaussian
Sinking velocity of POM, V_{POM} (m day^{-1})	0–100	0–100	Uniform
Global erosion/sedimentation rate, $f_{erosion}$ (normalized)[b]	0–0.5	0–0.5	Uniform

[a]The modern value is 0.18 Tmol P $year^{-1}$. [b]$f_{erosion}$ = 1 for the present.

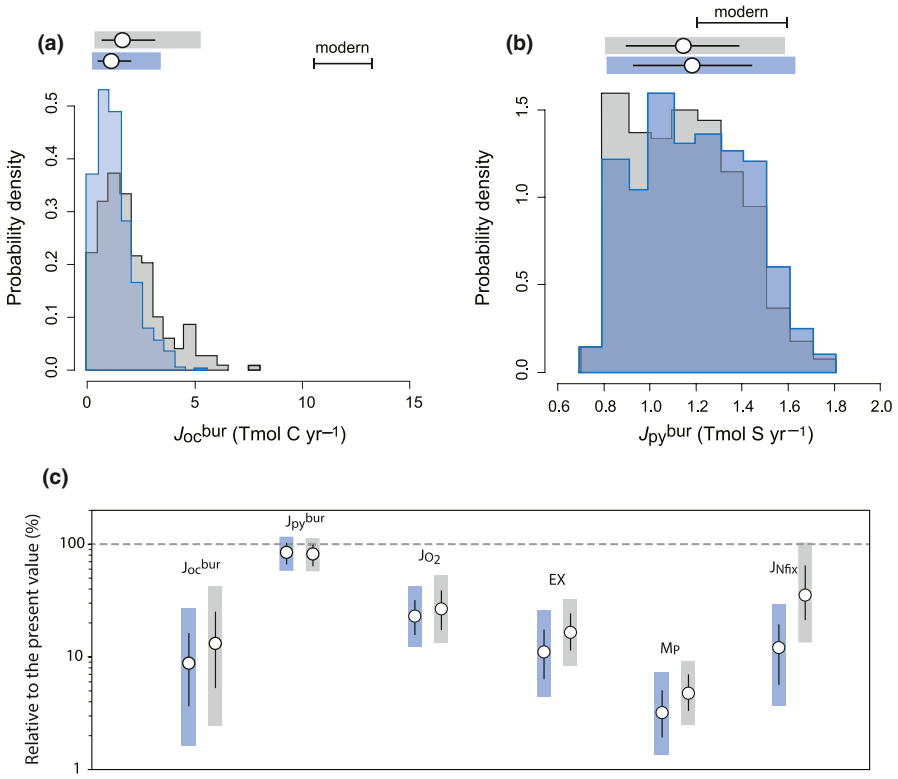

FIGURE 2 Posterior probability distributions retrieved by our model. The burial rates of organic carbon (J_{oc}^{bur}: a) and pyrite sulphur (J_{py}^{bur}: b) from our "Low O_2" (blue; n = 621) and "High O_2" (grey; n = 308) retrievals. Open circles represent median values. In both cases, error bar and grey-shaded region denote 1σ and 95% credible intervals, respectively. Double-headed arrows represent flux estimates for the modern or near-modern oceans. (c) Model retrieval of mid-Proterozoic Earth system biogeochemistry. J_{oc}^{bur} = burial rate of organic carbon. J_{py}^{bur} = burial rate of pyrite sulphur. J_{O2} = total rate of O_2 production. M_P = marine phosphate inventory. *EX* = export production of organic carbon. J_{Nfix} = rate of nitrogen fixation. All values are normalized to the modern or near-modern values [Colour figure can be viewed at wileyonlinelibrary.com]

with a 95% credible interval of 0.81–1.63 Tmol S year^{-1} (Figure 2b blue), within a factor of 2 of the "near-modern" (Quaternary average) ocean value of 1.2–1.6 Tmol S year^{-1} (Berner & Berner, 2012; Markovic, Paytan, & Wortmann, 2015). Taken together, we estimate a combined rate of O_2 production of about 3.51 Tmol O_2 year^{-1}, roughly 25% of the present value (J_{O2} in Figure 2c). We also find that the posterior distributions are largely unchanged for the "High O_2" scenario (Figure 2a,b grey) in which a possible range of the atmospheric O_2 levels is set to 1%–10% PAL (Table 1); in this case, the median value of J_{oc}^{bur} and total O_2 production rate are $1.64^{+1.52}_{-0.98}$ Tmol C year^{-1} and $4.06^{+1.91}_{-1.40}$ Tmol year^{-1}, respectively. Our model design is such that these are most likely upper limits (Supplementary information Methods).

Previous work has highlighted the issue of maintaining low O_2 fluxes in a pervasively reducing mid-Proterozoic ocean (Derry, 2015; Laakso & Schrag, 2014), given the enhanced preservation of organic matter in anoxic marine sediments (e.g., Katsev & Crowe, 2015). In our model, as in others (Laakso & Schrag, 2014; Reinhard et al., 2017), this can be attributed to strongly suppressed biological productivity (*EX* in Figure 2c). Given constraints on seawater [SO_4^{2-}], our model requires MSR to be suppressed by decreasing the availability of organic matter for MSR, and this can be achieved by a suppression of biological productivity through a scarcity of the primary nutrient (phosphorus, P) in the ocean interior (M_P in Figure 2c)—our model indicates that the marine P inventory would have been <10% of the present oceanic level (POL), with a median estimate of $3.2^{+1.9}_{-1.3}$% POL (1σ) and a 95% credible interval of 1.4%–7.3% POL for our "Low O_2" scenario. Our estimate of the deep water phosphate concentration of ~0.1 μM (Figure 3a) is within the range of 0.04–0.13 μM proposed by Jones et al. (Jones, Nomosatryo, Crowe, Bjerrum, & Canfield, 2015) from the P/Fe ratios of iron-rich chemical sediments deposited during the late Paleoproterozoic, but is based on a completely independent geologic constraint and implies that this condition extended well into the mid-Proterozoic.

However, we note that for our "Low O_2" scenario biological productivity may also have been impacted by increased solar UV flux because total O_3 column depth decreases significantly below 1% PAL (Segura et al., 2003). Our model does not account for this possible harmful effect of UV on life. On the other hand, UV fluxes attenuate rapidly with depth in seawater, with typical 10% depths for DNA damage well below 10 m in open ocean and coastal marine systems (Tedetti & Sempéré, 2006). In any case, our overarching result—strongly suppressed marine new production—would only be reinforced by the impact of increased solar UV flux. We also note that our model estimates a broadly similar M_P at $4.8^{+2.2}_{-1.4}$% POL (1σ) for our "High O_2" scenario, under which increased UV flux is not expected to play a significant role.

3.2 | The mid-Proterozoic Earth system

Our model retrieval provides statistical constraints on a number of major Earth system processes during the mid-Proterozoic. First, we estimate that the global rate of nitrogen fixation in mid-Proterozoic oceans was substantially lower than the present value: Our model predicts a globally integrated N fixation rate of 21^{+13}_{-11} Tg N year^{-1} (1σ) with a 95% credible interval of 6.5–52 Tg N year^{-1}. This value is a factor of ~7 below that estimated for the modern ocean (Eugster & Gruber, 2012; Groszkopf et al., 2012) (J_{Nfix} in Figure 2c) and arises

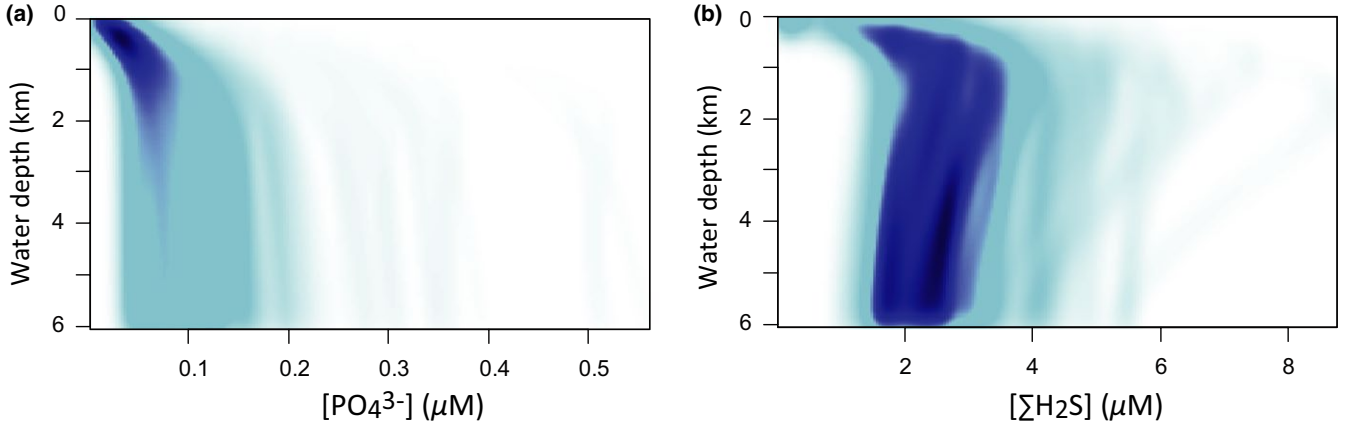

FIGURE 3 Chemistry of the ocean interior on the mid-Proterozoic Earth. Probability distribution of phosphate (left; a) and total sulphide (right; b) in the low–mid-latitude region for our "Low O_2" retrieval. Frequency is shown in colour contours. Note that although some coastal marine settings would likely deviate above these concentrations, in general, these are likely upper limits (see text) [Colour figure can be viewed at wileyonlinelibrary.com]

straightforwardly from suppressed N loss via denitrification in the nitrate-lean and oligotrophic oceans such that very little biological nitrogen fixation is required to meet the nutrient N demands of the biosphere. The broader implication is that any long-term trace nutrient deficiency acting at a global scale on the mid-Proterozoic Earth (Anbar & Knoll, 2002; Reinhard et al., 2013; Scott et al., 2008) would need to have been very extreme to be the ultimate limiting factor on O_2 fluxes from the biosphere, consistent with a recently emerging view of the factors regulating Earth's oxygenic biosphere through time (Laakso & Schrag, 2018; Reinhard et al., 2017).

Second, limited organic matter production provides a simple explanation for the accumulated geochemical data indicating that euxinic waters have been a predominantly local phenomenon for most of Earth's history (Planavsky et al., 2011; Poulton & Canfield, 2011; Reinhard et al., 2013). We estimate relatively low total sulphide (ΣH_2S) concentrations in the ocean interior, with our retrieval yielding values on the order of ~1 to 3 μM for the abyssal oceans (Figure 3b). It is important to bear in mind that this value is effectively a zonal/meridional average at each depth in our model such that deepwater H_2S concentrations well above this value are possible locally, particularly in coastal marine environments. On the other hand, the lack of a fully explicit Fe cycle in our model currently prevents us from diagnosing deep ocean [Fe^{2+}], and it is likely that for large regions of the ocean interior H_2S concentrations would be essentially negligible. Taken together, our results are consistent with the mid-Proterozoic global oceanic redox landscape inferred from geologic archives—globally ferruginous and locally euxinic (Planavsky et al., 2011; Poulton & Canfield, 2011)—and further suggest that this redox structure was controlled largely by limited flux of organic matter to the abyssal ocean (Planavsky et al., 2011; Poulton & Canfield, 2011; Reinhard et al., 2013; Scott et al., 2008). More granular constraints on the ocean redox landscape of the mid-Proterozoic Earth will require the development of more explicit Fe cycling in both low-order models like CANOPS and Earth system models of intermediate complexity (EMIC; (Claussen et al., 2002)).

Third, our model retrieves relatively low atmospheric CH_4 mixing ratios due to suppression of methanogenesis and concomitant degassing of CH_4 from the ocean to the atmosphere (Figure 4a,b). This can be attributed to the combined effect of limited organic matter availability for methanogenesis and aerobic and anaerobic CH_4 oxidation by O_2 and SO_4^{2-} (AOM), respectively (Olson, Reinhard, & Lyons, 2016). We estimate median values of ~3.4 ppmv and ~13.2 ppmv for our "Low O_2" and "High O_2" scenarios, slightly higher than the present value by a factor of 2–7 and consistent with recent estimates from 3-D ocean biogeochemical models both with and without AOM (Daines & Lenton, 2016; Olson et al., 2016). Relatively low atmospheric CH_4 levels during the mid-Proterozoic reinforce recent suggestions (Olson et al., 2016) that CH_4 and CO_2 alone may not have been sufficient to buffer the mid-Proterozoic climate system, unless terrestrial and/or abiotic CH_4 sources were much greater than at present (Zhao, Reinhard, & Planavsky, 2017). Moreover, low CH_4 mixing ratios in the atmosphere indicate a limited role of hydrogen escape to space in the mid-Proterozoic O_2 balance (see below).

Lastly, when we calculate the relative significance of pyrite burial and organic carbon burial in the O_2 production, our model shows that the rate of O_2 production via pyrite burial is comparable to, or larger than, organic carbon burial. We retrieve an O_2 production rate via pyrite burial that is ~1 to 8 times as large as the rate of O_2 production via organic carbon burial, with a median value of 2.2 for our "Low O_2" scenario (Figure 4c). Our "High O_2" scenario also estimates a median value of 1.4 with a 95% credible interval of 0.5–6.3. These represent a remarkable contrast to Earth system biogeochemistry during most of Phanerozoic time, during which organic carbon burial has represented the dominant O_2 source (Berner & Raiswell, 1983). Our result is consistent with an independent argument based on the geological record of carbon and sulphur isotopes (Canfield, 2005) and suggests that the sulphur cycle would have been a critical component of the global O_2 budget during the mid-Proterozoic.

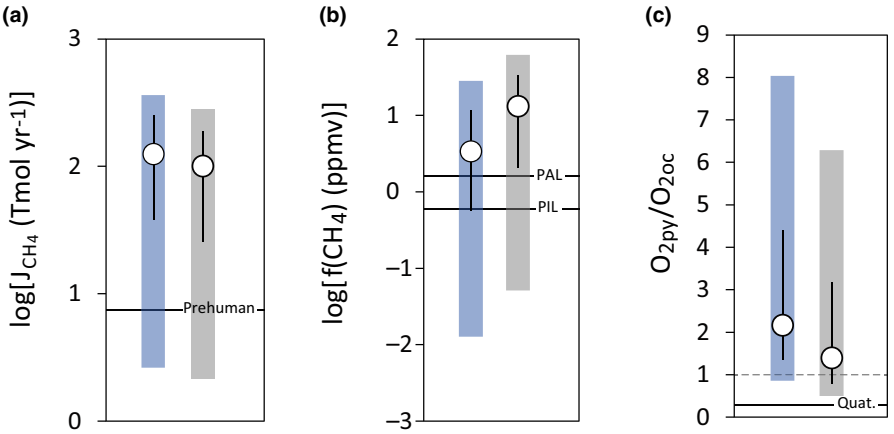

FIGURE 4 Model retrieval of mid-Proterozoic Earth system biogeochemistry for our "Low O_2" (blue) and "High O_2" (grey) scenarios. Open circles represent median values, while error bars and shaded regions represent 1σ and 95% credible intervals, respectively. (a) Degassing flux of CH_4 from the ocean to the atmosphere, the prehuman biospheric flux depicted as a horizontal solid line. (b) Atmospheric mixing ratio of CH_4. Preindustrial (PIL) and present (PAL) values are shown as horizontal solid lines. (c) Relative O_2 fluxes from pyrite sulphur burial (O_{2py}) and organic carbon burial (O_{2oc}). The Quaternary value depicted as a horizontal solid line [Colour figure can be viewed at wileyonlinelibrary.com]

TABLE 2 Reductant input rates required for the global O_2 balance

	Present[a]		Mid-Proterozoic (Low O_2 scenario)	Mid-Proterozoic (High O_2 scenario)
Species	Flux [Tmol year^{-1}]	Weighted flux [Tmol O_2 equiv. year^{-1}]	Weighted flux [Tmol O_2 equiv. year^{-1}]	Weighted flux [Tmol O_2 equiv. year^{-1}]
SO_2	0.63	0.315	0.315[b]	0.315[b]
H_2S	0.07 (Subaerial)	0.14	0.14[b]	0.14[b]
	0.10 (Submarine)	0.20	0.20[b]	0.20[b]
H_2	1.4	0.7	Φ_{out}(Red) = 2.09[c]	Φ_{out}(Red) = 0.19[c]
CO	0.1	0.05		
CH_4	<0.3	<0.6		
Fe^{2+}	0.3	0.075		
Total		1.48–2.08	2.75	0.85

[a]From Catling and Kasting (Catling and Kasting, 2017). [b]Present values are assumed for sulphur species (see Supporting information Methods). [c]From Supporting information equation S43.

3.3 | A global redox budget for the mid-Proterozoic

By embedding our estimates of O_2 production in a global redox balance framework (see Supporting information Methods), we can estimate the reductant fluxes from Earth's interior required to balance the global O_2 cycle across the range of parameters explored here (Table 2). We use a previously published parameterization for O_2 consumption associated with the oxidative weathering of organic matter (Daines, Mills, & Lenton, 2017; Lasaga & Ohmoto, 2002) (Supporting information equation S44) and ferrous iron (Kanzaki & Murakami, 2016; Yokota, Kanzaki, & Murakami, 2013) (Supporting information equation S45) (see Supporting information Methods), combined with the O_2 production fluxes derived above, to estimate that an external reductant flux of 2.75 Tmol O_2 equivalents year^{-1} is required to satisfy global redox balance under the mid-Proterozoic Earth system state retrieved by our model for our "Low O_2" scenario (Figure 5a). This can be compared to a modern reductant flux to Earth's surface from volcanism, hydrothermal systems and geologic/thermogenic CH_4 production of 1.5–2.1 Tmol O_2 equivalents year^{-1}. Given that even the modern solid Earth reductant flux cannot be constrained with a precision better than ~1 Tmol O_2 equivalents year^{-1}, it is clear that our "Low O_2" retrieval is fully consistent with a closed, stable redox balance. This is also true for our "High O_2" retrieval, in which 0.85 Tmol O_2 equivalents year^{-1} is sufficient to close the global redox budget (Table 2 and Figure 5b).

3.4 | Implications for the carbon isotope record

Geologic records of the carbon isotope composition of sedimentary carbonate rocks have often been used to estimate the relative

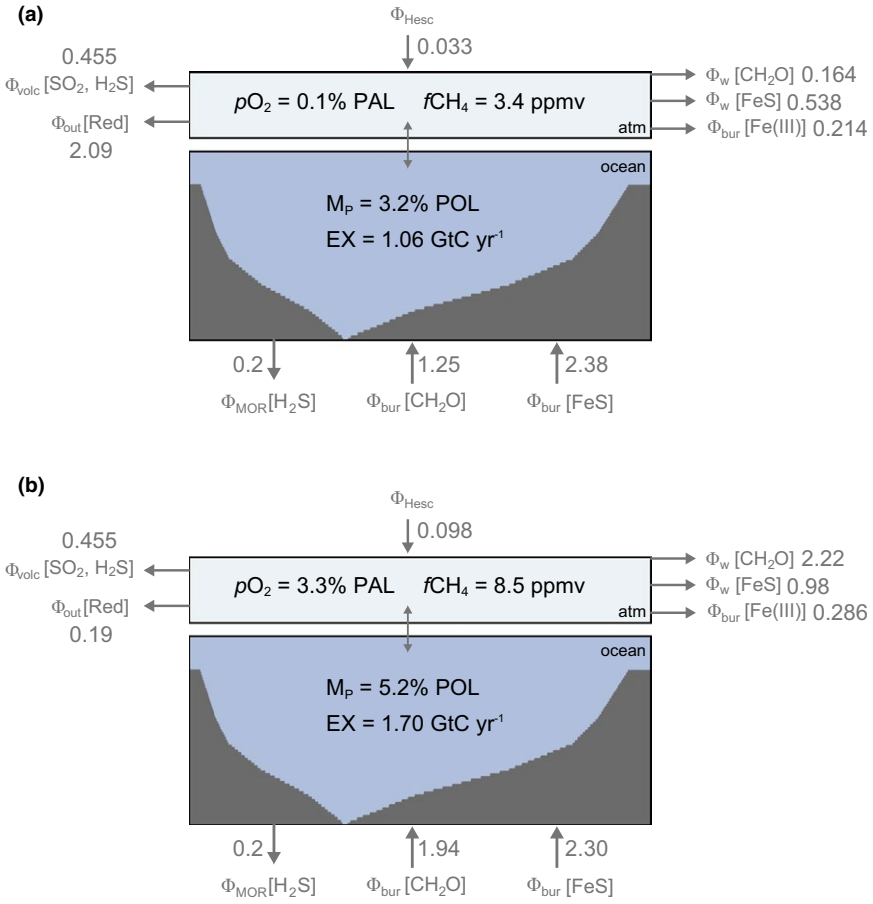

FIGURE 5 Global redox budget analysis from our Monte Carlo analysis for our "Low O_2" scenario (top: a) and "High O_2" scenario (bottom: b) of Proterozoic Earth surface system. Φ represents the mean value of the flow of oxidizing power in the system in terms of Tmol O_2 equivalents $year^{-1}$. $\Phi_{bur}(CH_2O)$ and $\Phi_{bur}(FeS)$ represent the input of oxidizing power via burial of organic matter and pyrite sulphur. Φ_{Hesc} denotes the flux of hydrogen escape to space, and "w" is the oxidative weathering. $\Phi_{MOR}(H_2S)$ and $\Phi_{volc}(SO_2, H_2S)$ are the output of oxidizing power via input of reduced sulphur gases through volcanic activity, which are treated as a free parameter [Colour figure can be viewed at wileyonlinelibrary.com]

fraction of carbon removed from the exogenic (ocean–atmosphere) system that is buried as organic carbon (f_{org}) (Broecker, 1970; Des Marais, Strauss, Summons, & Hayes, 1992; Hayes & Waldbauer, 2006; Krissansen-Totton et al., 2015; Kump & Arthur, 1999; Schidlowski, 1988). Canonically, this approach has been used to suggest that the relative organic matter burial fraction has not changed significantly throughout Earth's history. In principle, this represents a challenge to models that invoke suppressed marine organic matter production and burial, given that overall rates of carbon flow through the exogenic system would have to change dramatically and in concert with changes in organic carbon productivity/burial in order to maintain a stable f_{org}. However, this analysis assumes that the geological carbon cycle is in steady state and that the carbon isotopic composition ($\delta^{13}C$) of the overall input to the exogenic system is identical to the canonical mantle value of −5‰, when in reality this parameter should scale with atmospheric O_2 as a result of O_2-dependent changes to the globally integrated rates of organic carbon weathering in the crust (e.g., Bolton, Berner, & Petsch, 2006).

In contrast, our model predicts that oxidative weathering of organic matter would have been suppressed under mid-Proterozoic conditions, consistent with a number of recent models (Daines et al., 2017; Miyazaki, Planavsky, Bolton, & Reinhard, 2018). This results in $\delta^{13}C$ values for the integrated carbon flux to the ocean–atmosphere system that are significantly higher than the canonical mantle value (−0.3‰ and −1.1‰ for our "Low O_2" and "High O_2" scenarios, respectively; Supporting information Table S8). When combined with rates of volcanic CO_2 outgassing from the mantle (J_{mantle}) and carbonate weathering ($J_{carb}{}^{W}$) that are 150% of the reference values ($J_{mantle}{}^{*}$ = 2 Tmol C $year^{-1}$ and $J_{carb}{}^{*}$ = 40 Tmol C $year^{-1}$ where * denotes the reference value), we estimate f_{org} values of 1.2% and 4.3% for our "Low O_2" and "High O_2" scenarios, respectively (Supporting information Table S8), compared to a canonical value of ~15% to 20% (e.g., Krissansen-Totton et al., 2015). These results add to a growing body of work indicating that the quantitative scaling between the $\delta^{13}C$ values of marine sedimentary carbonate rocks and organic carbon burial fluxes from the exogenic system is somewhat obscure, particularly at low atmospheric pO_2 (Bjerrum & Canfield, 2004; Daines et al., 2017; Miyazaki et al., 2018; Schrag et al., 2013). Our model retrieval of the mid-Proterozoic Earth system is thus fully consistent with the existing carbon isotope record.

4 | CONCLUSION

In summary, our statistical analysis of a novel biogeochemical model indicates that the rate of O_2 production in mid-Proterozoic oceans was lower than that in the modern ocean by as much as an order of magnitude or more, providing a compelling mechanism for explaining the protracted oxygenation of the Earth's atmosphere. We estimate the residence time of O_2 in the combined ocean–atmosphere system at ~10 to 300 kyr, implying either an intriguing but poorly understood series of rapid stabilizing feedbacks within the coupled carbon, nutrient and oxygen cycles at Earth's surface or the potential for significant oscillation in ocean–atmosphere O_2 on relatively short timescales. In any case, our results provide a comprehensive and statistically robust picture of the mid-Proterozoic Earth system that is fully consistent with both current understanding of the coupled C-N-P-O_2-S cycles and existing constraints from the geologic record, and a baseline from which to examine how and why secular oxygenation of Earth's ocean–atmosphere system occurred during the late Neoproterozoic.

ACKNOWLEDGMENTS

We are grateful to J. Kasting and E. Stueken for their constructive comments on early draft of this manuscript. This work was supported by JSPS KAKENHI Grant Number JP25870185 and JP16K05618. K.O. acknowledges support from the NASA Postdoctoral Program at the NASA Astrobiology Institute, administered by Universities Space Research Association under contact with NASA. C.T.R. acknowledges support from the NASA Astrobiology Institute, the National Science Foundation and the Alfred P. Sloan Foundation. The authors declare no competing financial interests.

ORCID

Kazumi Ozaki http://orcid.org/0000-0003-1121-8921

Eiichi Tajika http://orcid.org/0000-0001-6674-3147

REFERENCES

Anbar, A. D., & Knoll, A. H. (2002). Proterozoic ocean chemistry and evolution: A bioinorganic bridge? *Science*, *297*, 1137–1142.

Berner, R. A. (1982). Burial of organic carbon and pyrite sulfur in the modern ocean; its geochemical and environmental significance. *American Journal of Science*, *282*, 451–473.

Berner, E. K., & Berner, R. A. (2012). *Global environment: Water, air, and geochemical cycles*. Princeton, NJ: Princeton University Press.

Berner, R. A., & Raiswell, R. (1983). Burial of organic carbon and pyrite sulfur in sediments over phanerozoic time: A new theory. *Geochimica et Cosmochimica Acta*, *47*, 855–862.

Bjerrum, C. J., & Canfield, D. E. (2002). Ocean productivity before about 1.9 Gyr ago limited by phosphorus adsorption onto iron oxides. *Nature*, *417*, 159–162.

Bjerrum, C. J., & Canfield, D. E. (2004). New insights into the burial history of organic carbon on the early Earth. *Geochemistry, Geophysics, Geosystems*, *5*, Q08001.

Bolton, E. W., Berner, R. A., & Petsch, S. T. (2006). The weathering of sedimentary organic matter as a control on atmospheric O2: II. Theoretical Modeling. *American Journal of Science*, *306*, 575–615.

Broecker, W. S. (1970). A boundary condition on the evolution of atmospheric oxygen. *Journal of Geophysical Research*, *75*, 3553–3557.

Burdige, D. J. (2005). Burial of terrestrial organic matter in marine sediments: A re-assessment. *Global Biogeochemical Cycles*, *19*, GB4011.

Canfield, D. E. (2005). The early history of atmospheric oxygen: Homage to Robert M. Garrels. *Annual Review of Earth and Planetary Sciences*, *33*, 1–36.

Catling, D. C., & Kasting, J. F. (2017). *Atmospheric Evolution on Inhabited and Lifeless Worlds*. Cambridge, UK: Cambridge Univ. Press.

Claussen, M., Mysak, L., Weaver, A., Crucifix, M., Fichefet, T., Loutre, M.-F., … Wang, Z. (2002). Earth system models of intermediate complexity: Closing the gap in the spectrum of climate system models. *Climate Dynamics*, *18*, 579–586.

Cole, D. B., Reinhard, C. T., Wang, X., Gueguen, B., Halverson, G. P., Gibson, T., … Planavsky, N. J. (2016). A shale-hosted Cr isotope record of low atmospheric oxygen during the Proterozoic. *Geology*, *44*, 555–558.

Daines, S. J., & Lenton, T. M. (2016). The effect of widespread early aerobic marine ecosystems on methane cycling and the Great Oxidation. *Earth and Planetary Science Letters*, *434*, 42–51.

Daines, S. J., Mills, B. J. W., & Lenton, T. M. (2017). Atmospheric oxygen regulation at low Proterozoic levels by incomplete oxidative weathering of sedimentary organic carbon. *Nature Communications*, *8*, 14379.

Derry, L. A. (2015). Causes and consequences of mid-Proterozoic anoxia. *Geophysical Research Letters*, *42*, 2015GL065333.

Des Marais, D. J., Strauss, H., Summons, R. E., & Hayes, J. M. (1992). Carbon isotope evidence for the stepwise oxidation of the Proterozoic environment. *Nature*, *359*, 605.

Eugster, O., & Gruber, N. (2012). A probabilistic estimate of global marine N-fixation and denitrification. *Global Biogeochemical Cycles*, *26*, GB4013.

Fiebig, J., Woodland, A. B., D'Alessandro, W., & Püttmann, W. (2009). Excess methane in continental hydrothermal emissions is abiogenic. *Geology*, *37*, 495–498.

Goldblatt, C., Lenton, T. M., & Watson, A. J. (2006). Bistability of atmospheric oxygen and the Great Oxidation. *Nature*, *443*, 683–686.

Groszkopf, T., Mohr, W., Baustian, T., Schunck, H., Gill, D., Kuypers, M. M. M., … LaRoche, J. (2012). Doubling of marine dinitrogen-fixation rates based on direct measurements. *Nature*, *488*, 361–364.

Hardisty, D. S., Lu, Z., Bekker, A., Diamond, C. W., Gill, B. C., Jiang, G., … Lyons, T. W. (2017). Perspectives on Proterozoic surface ocean redox from iodine contents in ancient and recent carbonate. *Earth and Planetary Science Letters*, *463*, 159–170.

Hayes, J. M., & Waldbauer, J. R. (2006). The carbon cycle and associated redox processes through time. *Philosophical Transactions of the Royal Society B*, *361*, 931–950.

Holland, H. D. (1984). *The Chemical Evolution of the Atmosphere and Oceans*. Princeton: Princeton University Press.

Jones, C., Nomosatryo, S., Crowe, S. A., Bjerrum, C. J., & Canfield, D. E. (2015). Iron oxides, divalent cations, silica, and the early earth phosphorus crisis. *Geology*, *43*, 135–138.

Kah, L. C., Lyons, T. W., & Frank, T. D. (2004). Low marine sulphate and protracted oxygenation of the Proterozoic biosphere. *Nature*, *431*, 834–838.

Kanzaki, Y., & Murakami, T. (2016). Estimates of atmospheric O_2 in the Paleoproterozoic from paleosols. *Geochimica et Cosmochimica Acta*, *174*, 263–290.

Katsev, S., & Crowe, S. A. (2015). Organic carbon burial efficiencies in sediments: The power law of mineralization revisited. *Geology*, *43*, 607–610.

Krissansen-Totton, J., Buick, R., & Catling, D. C. (2015). A statistical analysis of the carbon isotope record from the Archean to Phanerozoic

and implications for the rise of oxygen. *American Journal of Science*, *315*, 275–316.
Kump, L. R. (2008). The rise of atmospheric oxygen. *Nature*, *451*, 277–278.
Kump, L. R., & Arthur, M. A. (1999). Interpreting carbon-isotope excursions: Carbonates and organic matter. *Chemical Geology*, *161*, 181–198.
Laakso, T. A., & Schrag, D. P. (2014). Regulation of atmospheric oxygen during the Proterozoic. *Earth and Planetary Science Letters*, *388*, 81–91.
Laakso, T. A., & Schrag, D. P. (2018). Limitations on limitation. *Global Biogeochemical Cycles*, *32*, 486–496.
Lasaga, A. C., & Ohmoto, H. (2002). The oxygen geochemical cycle: Dynamics and stability. *Geochimica et Cosmochimica Acta*, *66*, 361–381.
Luo, G., Ono, S., Huang, J., Algeo, T. J., Li, C., Zhou, L., … Xie, S. (2015). Decline in oceanic sulfate levels during the early Mesoproterozoic. *Precambrian Research*, *258*, 36–47.
Lyons, T. W., & Gill, B. C. (2010). Ancient sulfur cycling and oxygenation of the early biosphere. *Elements*, *6*, 93–99.
Lyons, T. W., Reinhard, C. T., & Planavsky, N. J. (2014). The rise of oxygen in Earth's early ocean and atmosphere. *Nature*, *506*, 307–315.
Markovic, S., Paytan, A., & Wortmann, U. G. (2015). Pleistocene sediment offloading and the global sulfur cycle. *Biogeosciences*, *12*, 3043–3060.
Miyazaki, Y., Planavsky, N., Bolton, E. W., & Reinhard, C. T. (2018). Making sense of massive carbon isotope excursions with an inverse carbon cycle model. *Journal of Geophysical Research: Biogeosciences*, *123*, 2485–2496.
Muller-Karger, F. E., Varela, R., Thunell, R., Luerssen, R., Hu, C., & Walsh, J. J. (2005). The importance of continental margins in the global carbon cycle. *Geophysical Research Letters*, *32*, L01602.
Olson, S. L., Reinhard, C. T., & Lyons, T. W. (2016). Limited role for methane in the mid-Proterozoic greenhouse. *Proceedings of the National Academy of Sciences of the United States of America*, *113*, 11447–11452.
Ozaki, K., & Tajika, E. (2013). Biogeochemical effects of atmospheric oxygen concentration, phosphorus weathering, and sea-level stand on oceanic redox chemistry: Implications for greenhouse climates. *Earth and Planetary Science Letters*, *373*, 129–139.
Ozaki, K., Tajima, S., & Tajika, E. (2011). Conditions required for oceanic anoxia/euxinia: Constraints from a one-dimensional ocean biogeochemical cycle model. *Earth and Planetary Science Letters*, *304*, 270–279.
Planavsky, N. J., Bekker, A., Hofmann, A., Owens, J. D., & Lyons, T. W. (2012). Sulfur record of rising and falling marine oxygen and sulfate levels during the Lomagundi event. *Proceedings of the National Academy of Sciences of the United States of America*, *109*, 18300–18305.
Planavsky, N. J., McGoldrick, P., Scott, C. T., Li, C., Reinhard, C. T., Kelly, A. E., … Lyons, T. W. (2011). Widespread iron-rich conditions in the mid-Proterozoic ocean. *Nature*, *477*, 448–451.
Planavsky, N. J., Reinhard, C. T., Wang, X., Thomson, D., McGoldrick, P., Rainbird, R. H., … Lyons, T. W. (2014). Low Mid-Proterozoic atmospheric oxygen levels and the delayed rise of animals. *Science*, *346*, 635–638.
Planavsky, N. J., Rouxel, O. J., Bekker, A., Lalonde, S. V., Konhauser, K. O., Reinhard, C. T., & Lyons, T. W. (2010). The evolution of the marine phosphate reservoir. *Nature*, *467*, 1088–1090.
Poulton, S. W., & Canfield, D. E. (2011). Ferruginous conditions: A dominant feature of the ocean through earth's history. *Elements*, *7*, 107–112.
Reinhard, C. T., Planavsky, N. J., Gill, B. C., Ozaki, K., Robbins, L. J., Lyons, T. W., … Konhauser, K. O. (2017). Evolution of the global phosphorus cycle. *Nature*, *541*, 386–389.
Reinhard, C. T., Planavsky, N. J., Robbins, L. J., Partin, C. A., Gill, B. C., Lalonde, S. V., … Lyons, T. W. (2013). Proterozoic ocean redox and biogeochemical stasis. *Proceedings of the National Academy of Sciences of the United States of America*, *110*, 5357–5362.
Schidlowski, M. (1988). A 3,800-million-year isotopic record of life from carbon in sedimentary rocks. *Nature*, *333*, 313.
Schrag, D. P., Higgins, J. A., Macdonald, F. A., & Johnston, D. T. (2013). Authigenic carbonate and the history of the global carbon cycle. *Science*, *339*, 540–543.
Scott, C., Lyons, T. W., Bekker, A., Shen, Y., Poulton, S. W., Chu, X., & Anbar, A. D. (2008). Tracing the stepwise oxygenation of the Proterozoic ocean. *Nature*, *452*, 456–459.
Scott, C., Wing, B. A., Bekker, A., Planavsky, N. J., Medvedev, P., Bates, S. M., … Lyons, T. W. (2014). Pyrite multiple-sulfur isotope evidence for rapid expansion and contraction of the early Paleoproterozoic seawater sulfate reservoir. *Earth and Planetary Science Letters*, *389*, 95–104.
Segura, A., Krelove, K., Kasting, J. F., Sommerlatt, D., Meadows, V., Crisp, D., … Mlawer, E. (2003). Ozone concentrations and ultraviolet fluxes on earth-like planets around other stars. *Astrobiology*, *3*, 689–708.
Tang, D., Shi, X., Wang, X., & Jiang, G. (2016). Extremely low oxygen concentration in mid-Proterozoic shallow seawaters. *Precambrian Research*, *276*, 145–157.
Tedetti, M., & Sempéré, R. (2006). Penetration of ultraviolet radiation in the marine environment. A Review. *Photochemistry and Photobiology*, *82*, 389–397.
Wallmann, K., Pinero, E., Burwicz, E., Haeckel, M., Hensen, C., Dale, A., & Ruepke, L. (2012). The global inventory of methane hydrate in marine sediments: A theoretical approach. *Energies*, *5*, 2449.
Yokota, K., Kanzaki, Y., & Murakami, T. (2013). Weathering model for the quantification of atmospheric oxygen evolution during the Paleoproterozoic. *Geochimica et Cosmochimica Acta*, *117*, 332–347.
Zhao, M., Reinhard, C. T., & Planavsky, N. J. (2017). Terrestrial methane fluxes and Proterozoic climate. *Geology*, *46*, 139–142.

SUPPORTING INFORMATION

Additional supporting information may be found online in the Supporting Information section at the end of the article.

How to cite this article: Ozaki K, Reinhard CT, Tajika E. A sluggish mid-Proterozoic biosphere and its effect on Earth's redox balance. *Geobiology*. 2019;17:3–11. https://doi.org/10.1111/gbi.12317